Volume 9, Issue 4, 2019, 3996 - 4005 ISSN 2069-5837

Biointerface Research in Applied Chemistry

www.BiointerfaceResearch.com

https://doi.org/10.33263/BRIAC94.996005

Original Research Article Open Access Journal

Received: 25.06.2019 / Revised: 29.07.2019 / Accepted: 04.08.2019 / Published on-line: 15.08.2019

Response surface methodology for optimization of Cd(II) adsorption from wastewaters by fabricated tartaric acid-maize tassel magnetic hybrid sorbent

Sithulisiwe Ngwenya [1], Upenyu Guyo [1,*], Ngceboyakwethu Primrose Zinyama [1], Fidelis Chigondo [1], Benias Chomunorwa Nyamunda [2], Netai Muchanyereyi [3]

[1]Department of Chemical Technology, Midlands State University, Senga Road, Gweru Zimbabwe
[2]Department of Chemical and Processing Engineering, Manicaland State University of Applied Sciences, Off-Vumba Road, Mutare, Zimbabwe
[3]Department of Chemistry, Bindura University of Science Education, Chimurenga Road, Bindura, Zimbabwe

*corresponding author e-mail address: ***guyou@staff.msu.ac.zw***

ABSTRACT

Maize tassels (MT), an agro-based biomass waste was carbonised followed by thermo-chemical modification using tartaric acid. The functionalized activated carbon was further modified to yield a magnetic hybrid composite adsorbent. The adsorbent was characterized using Fourier transform infrared (FTIR) spectroscopy, X-ray diffraction (XRD) and Scanning Electron Microscopy (SEM). The adsorbent was evaluated for its efficiency to remove Cd(II) ions from aqueous solutions through batch adsorption studies following a Central Composite Design. Effects of solution pH, contact time, adsorbent dosage, initial metal concentration and temperature on Cd(II) adsorption were investigated. Optimization of the adsorption process was done using desirability function on the Design Expert V11 software. The desirability function showed that the optimum parameters were pH 5.29, contact time (67.50 min), dosage (0.575 g) and initial concentration (152.50 mg/L). The adsorption process was analysed using kinetic and isotherm models. The kinetics of the adsorption process followed the pseudo-second-order model (lowest sum of square error (SSE) values and correlation coefficients (R^2) > 0.999) in addition to the intraparticle diffusion model. The isotherm data were consistent with the Langmuir isotherm as evidenced by the highest correlation coefficient (R^2 = 0.998). The thermodynamic parameters showed that the process was endothermic and spontaneous in nature. The adsorption capacity of the adsorbent was found to be 188.68 mg/g at 20 ºC which is higher than that of the previously reported magnetic maize tassel hybrid (52.05 mg/g). The adsorbent showed good removal efficiency on real effluent samples.

Keywords: *Tartaric acid-maize tassel magnetic hybrid; Cd(II) adsorption; response surface methodology, isotherm.*

1. INTRODUCTION

Safe water is a basic necessity in the development of plant, animal and human societies. Shortage of potable water stunts the development of societies and induces a threat in the general survival of human mankind. The development and promotion of industrial activities have contributed vastly to heavy metal contamination in ground and surface water [1]. Heavy metals such as cadmium, lead, arsenic and mercury even at trace levels in water pose adverse health effects as they are persistent, toxic and non-degradable. Their non-degradability traits result in accumulation of the metals through the food chain [2, 3].

Among the toxic heavy metals, bivalent cadmium (Cd(II)), a heavy and toxic metal has attracted much attention in environmental research as it greatly affects human beings, flora and fauna [4]. In addition to the abovementioned effects, Cd is a carcinogen, tetragen and potent enzyme inhibitor which cause effects including cancer, hypertension, renal disturbances, polymenia and multiple organ failure in humans [5]. The World Health Organisation recommends that Cd(II) in drinking water should not exceed 0.005 mg/L [6]. Removal of Cd(II) from water systems should therefore be given high priority.

Many technologies including precipitation, electrochemical, solvent extraction, ion exchange, membrane separation, etc, have been explored for Cd(II) removal [7, 8]. However, their use is limited by a number of demerits they possess which include high operation costs, complicated operation and incomplete metal removal [3, 9, 10]. Relative to the aforementioned technologies, adsorption has advantages such as ease of operation, effectiveness and reversibility which enables regeneration and reusability of the spent adsorbent material.

A number of materials have been fabricated and explored for their capability to remove Cd(II) from wastewaters. These adsorbents include activated carbon [10, 11], carbon nanotubes [12-14], magnetite hybrids [11, 15-18], biopolymers [8], and polymers [19,20]. In our previous studies, we explored the use of maize tassels and showed that it can be used as a precursor in the fabrication of potential adsorbents for removing Cd(II) ions from wastewaters [21]. The maximum adsorption capacity obtained was however unsatisfactory and could be improved. The situation led us to consider the fabrication of maize tassel nanohybrid composites [16]. This technology showed enhanced Cd(II) removal relative to the former though could be better. This prompted the synthesis of maize tassel-methyl methacrylate biopolymers which showed an improved Cd(II) ions removal efficiency.

Activated carbons which belong to a group of microporous materials have been used extensively to remove various contaminants, both organic and inorganic either in liquid or gaseous state from the environment [22]. Activated carbon (AC) has an amorphous structure with well-defined pore structure, size and volume in addition to various heteroatoms that contribute to its outstanding and unique adsorption properties [23]. These

properties allow AC's surface characteristics to be modified to suit a specific application.

In this study, low-cost and abundant maize tassel biomass was used as a precursor to the novel agro-based adsorbent. Agro-based materials are rich sources of cellulose which are biodegradable and non-meltable [21]. The biomass was thermo-chemically modified with tartaric acid and then materialized to yield a magnetite hybrid adsorbent. The prepared adsorbent was evaluated for its capability to remove Cd(II) from wastewaters. The adsorption behavior of Cd(II) was investigated with respect to solution pH, adsorbent dosage, initial concentration and contact time. These parameters were optimized collectively using a statistical technique, Response Surface Methodology (RSM). A RSM is a mathematical statistical technique which optimizes the process and evaluates the relationship between a set of independent variables for specific responses with a minimum number of planned experiments [24,25]. RSM evaluates the relative significance of the various independent variables in the presence of complex factor– factor interactions [26]. Furthermore, a response surface (a graphical representation) is obtained which may describe the effects of the parameters on the response variable [27]. Regeneration and reusability of the adsorbent were also evaluated following several cycles of adsorption-desorption studies. Consequently, the fabricated adsorbent was evaluated for its potential application in real effluent samples.

2. MATERIALS AND METHODS

2.1. Materials.

All chemicals were of AR grade and were used as received. Distilled water (Midlands State University laboratory), pulverized maize tassels activated carbon (Midlands State University laboratory), tartaric acid (99.5%, Skylabs), ferric chloride (99%, univAR), iron (II) chloride (99%, uni-CHEM), potassium bromide (99%, Associated Chemical Enterprises), sulphuric acid (32%, Glass world), ethane diamine (Skylabs), cadmium nitrate (99%, Labchem), hydrochloric acid (32%, Scientific Masters), sodium hydroxide (98%, Glass world).

2.2. Preparation of tartaric acid modified activated carbon (TAC).

Maize tassels were collected from a local farm in Gweru, Zimbabwe. The maize tassels were pretreated and carbonized as reported elsewhere [16,21]. To modify the activated carbon with tartaric acid, activated carbon (50 g) was mixed with 600 mL of 0.5 M tartaric acid. The mixture was subjected to 50 ^{o}C for 24 h. The temperature was raised to 120 ^{o}C for 90 min for a thermochemical reaction between the activated carbon and tartaric acid to occur. The heated material was then washed thoroughly with boiling distilled water and then soaked in NaOH (0.1 M) in a suitable ratio and stirred for 60 min. The residual alkali was removed by thoroughly washing the maize tassel until the residual solution had reached a pH of 7. The sample was dried to constant weight at 50 ^{o}C. The dry adsorbent was then preserved in a desiccator.

2.3. Synthesis of magnetic hybrid (TAC-MH) adsorbent.

The magnetic hybrid (MH) was prepared using methods reported elsewhere [3,28,29]. $FeCl_3.6H_2O$ (89.54 g; 505 mmol) $FeCl_2.4H_2O$ (44.77 g; 325 mmol) and TAC (40.70 g) were mixed in deionised (120 mL) water in a reaction vessel which was stirred at 80 ^{o}C. Ethane diamine (10 mL) was added drop wisely under nitrogen protection and mechanically stirred for 2 h. After the reaction, the solid particles were separated from the reaction medium using a magnet. The particles were then washed using water repeatedly with the use of a centrifuge. The particles were then dried under vacuum at 60 ^{o}C.

2.4. Characterization of the adsorbent. The selected physicochemical characteristics of the fabricated adsorbent such as particle size, bulk density, iodine number, total ash content and moisture content were determined using standard methods. The zero point charge (ZPC) of the adsorbent was determined by powder addition method [11,30]. A Thermofischer Scientific spectrometer (Nicolet 6700, USA) in the scanning range 4000 – 400 cm^{-1} was used to obtain the Fourier transform infrared spectroscopy (FTIR) spectra of the adsorbent. The structural phase of the adsorbent was identified using a Bruker D8 Advance X-ray diffractometer (Germany) using nickel filtered Cu Kαradiation (40 kV, 40 mA). A scanning electron microscope (SEM) JEOL model JSM-250 was used to obtain the morphologies and the surface structure of the adsorbent. The magnetic property of the fabricated adsorbent was demonstrated using a magnet.

2.5. Preparation of stock solution.

A stock solution of 1000 mg/L of metformin dihydrochloride (MH) was prepared by dissolving approximately 1.00 mg of analytical grade MH in 100 mL of distilled water. The used concentrations were obtained by serial dilution of the stock solution.

2.6. Batch adsorption studies.

The batch adsorption studies were carried out following the experimental design developed using the Design Expert V11 software by mixing appropriate amounts of adsorbent under specified conditions with 100 mL of Cd(II) solution. The solution pH was adjusted using 0.1 M HCl or 0.1 M NaOH. The mixture was shaken at 150 rpm on a shaker for a time stipulated in the design at room temperature. An external magnet was used to separate the adsorbent from the mixture solution. Analysis of residual Cd(II) ions in the supernatant liquid was carried out using flame atomic absorption spectrometer (FAAS, Shimadzu, AA-6800). The Cd(II) percentage removal (R) was calculated according to Equation 1.

$$R = \frac{(C_o - C_e)}{C_o} \times 100\% \quad (1)$$

The adsorption amount (q_e) was determined using Equation 2:

$$q_e = \frac{(C_o - C_e)V}{M} \quad (2)$$

where q_e is the amount (mg/g) of Cd(II) ions adsorbed, C_0 and C_e are the Cd(II) concentrations (mg/L) in the solution initially and

after adsorption, respectively, V is the volume (L) of the solution, and M is the mass (g) of adsorbent used in the experiment.

2.7. Experimental design.

A version 11 of the Design Expert software was used to model the experimental design of the adsorption process. An experimental domain (Table 1) was derived after running a few preliminary ad hoc batch experiments. A full central composite design (CCD) was employed to investigate the influences of pH (2 - 8), contact time (5 - 240 min), adsorbent dosage (0.1 – 1.2 g) and initial Cd(II) concentration (5 - 100 mg/L) on Cd(II) ions removal from aqueous solution. The adsorption capacity was taken as the response variable. Optimization of the levels of process variables, statistical, regression and graphical analysis of the data obtained were done using the Design Expert version 11 software. The proposed quadratic model for the adsorption process was modelled to be:

$$q_e = \beta_0 + \beta_1 A + \beta_2 B + \beta_3 C + \beta_4 D + \beta_5 A^2 + \beta_6 B^2 + \beta_7 C^2 + \beta_8 D^2 + \beta_9 AB + \beta_{10} AC + \beta_{11} AD + \beta_{12} BC + \beta_{13} BD + \beta_{14} CD \quad (3)$$

where q_e is the adsorption capacity, A is the pH, B is the contact time in min, C is the dosage in g and D is the initial concentration in mg/L.

2.8. Error analysis. The kinetic models were assessed for fitness by the square sum of error (SSE) test. A lower SSE test values show that the model best describes the kinetics of the adsorption process. Equation 4 was used to calculate SSE:

$$\text{SSE} = \sum_{i=1}^{n} \left(\frac{(q_{t,e} - q_{t,m})}{{q_{t,e}}^2} \right)^2 \quad (4)$$

Where $q_{t,e}$ and $q_{t,m}$ are the experimental adsorption capacities of Cd(II) ions in mg/g at time t and the corresponding values obtained from the kinetic models.

2.9. Desorption studies.

Desorption experiments were conducted using NaOH as the eluent. The concentration of NaOH was optimized by varying NaOH concentrations (0.05 -0.4 M) in desorbing Cd(II) ions from spent adsorbent material. The optimum NaOH concentration was deduced to be 0.1 M. Briefly, 50 mL of specified NaOH concentration was added to a pre-weighed used adsorbent. The mixture was agitated on a shaker at 150 rpm for 60 min at room temperature. The mixture was then filtered and the supernatant liquid was analzsed for the desorbed metal ions. The generated adsorbent was used again in an adsorption experiment to evaluate whether it could be used again. The adsorption-desorption cycles were repeated 5 times to evaluate the regeneration and reusability of the adsorbent.

3. RESULTS

3.1. Characterization of the adsorbent.

3.1.1. Physicochemical properties of the adsorbent. Selected physicochemical properties of TAC-MH were determined. The adsorbent was screened using a sieve to get particles sizes of less than 100 µm for use in the adsorption process. Smaller adsorbent particle sizes provide a larger surface area for exposure to the adsorbate which enhances the adsorption efficiency of the adsorbent. Though a low moisture content does not affect the adsorption power of the adsorbent, it favors the adsorption process since the dilution effect on the action of adsorbent is minimised [21]. In the present study, the moisture content was 3.21% implying that it had a poor affinity for water and hence the dilution effect could not affect the adsorption process. A higher moisture content may demand an additional weight of the adsorbent during the adsorption process. The total ash content of the adsorbent was determined to be 2.86%, implying it could have good adsorption efficiency towards Cd(II) ions [31,32]. The bulk density of TAC-MH was 0.83 mg/L indicating its suitability for the adsorption process.

3.1.2. FTIR characterization. Fig. 1 shows the FT-IR spectra for activated carbon (a), tartaric acid modified activated carbon (b) and the magnetite hybrid activated carbon (c). The FTIR spectra were employed to evaluate the success of subsequent modifications of the maize tassel activated carbon. The FTIR spectra showed presence of carboxyl, hydroxyl and amide groups in the adsorbent. The peaks at 3228 and 3417 cm^{-1} are characteristic of OH and NH stretching vibrations of polymeric compounds whilst the bands at 2924 cm^{-1} are stretching vibrations of carboxylic acid CH groups. The peak at 1572.99 cm^{-1} is in the region of 1300-1750 cm^{-1}, which comprises amides, aromatic C=C stretching vibration and aliphatic C-H asymmetric and symmetric bending vibrations [33]. The peak at 1739.21 cm^{-1} shows the presence of C=O stretching bond which is a functional group of carboxylic acids and is usually observed in raw materials [33, 34]. The peak at 1143.58 cm^{-1} is a very large peak related to ash composition [33], it shows C-O stretching of alcohols, ethers or hydroxyl groups [34]. The region 675-900 cm^{-1} consists of C-H bonds that show the presence of aromatics on the surface of the material and two peaks were found in that region at 808.46 and 876.25 cm^{-1}.

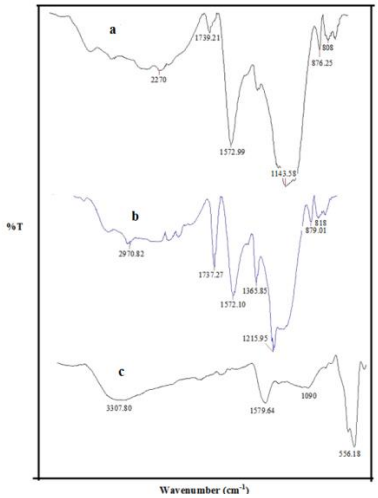

Figure. 1. FTIR spectra of maize tassel activated carbon (a), tartaric acid modified activated (b) and magnetite tartaric acid modified activated carbon (c).

The increase in the intensity of the peak formed at 1737.27 cm^{-1} (Fig 1b) confirms the success of tartaric acid modification of activated carbon [33]. The magnetite tartaric acid modified activated carbon shows a broad peak at 3307.80 cm^{-1} (Fig 1c). This peak is assigned to the stretching of the O-H of alcohols, phenols or carboxylic acids due to intermolecular and intramolecular hydrogen binding of the activated carbon [34]. The peak at 1090.35 cm^{-1} is associated with the C=O stretch which

shows the presence of carboxylic groups on the surface of the adsorbent. The presence of Fe-O band at 556.18 cm^{-1} shows the presence of magnetic nanoparticles that were incorporated during the synthesis of the adsorbent.

3.1.3, XRD analysis. X-ray diffraction patterns of maize tassel activated carbon (a) and the magnetite hybrid adsorbent (b) are presented in Fig 2. Fig 2a shows a continuous function with a broad peak at around $2\theta = 20^{o}$ which is typical of diffraction pattern of an amorphous material. Fig 2b shows peaks at 2θ = 33°, 37°, 42°, 54°, 59°, and 62° corresponding to (220), (311), (400), (422), (440) and (511) Bragg reflection, respectively [11,28] characteristic of iron oxide magnetic particles in the prepared adsorbent.

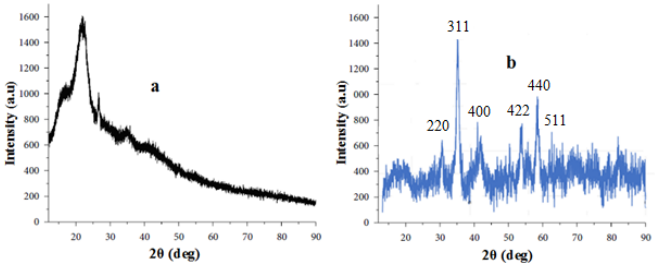

Figure. 2. XRD spectra of maize tassel activated carbon (a) and magnetite tartaric acid modified activated carbon (TAC-MH) (b).

3.1.4. SEM-EDX. Further evidence for successful modification of maize tassel activated carbon is presented by EDX micrographs in Fig 3. Fig 3a shows the presence of silicon, oxygen, phosphorus and an intense carbon peak on the surface of the material characteristic of activated carbon. An increase in the intensity of the oxygen peak is witnessed in Fig 3b attributed to tartaric acid modification of activated carbon. Presence of iron and oxygen in Fig 3c provides proof for successful embedment of magnetite nanoparticles in the tartaric acid modified activated carbon mass.

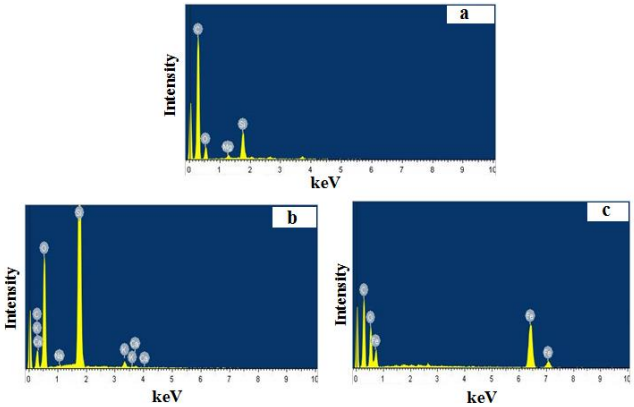

Figure 3. SEM micrographs for maize tassel activated carbon (a) and magnetite tartaric acid modified activated carbon (b).

3.2. Batch adsorption studies.

The experimental domain used to build a central composite design which was employed on batch adsorption studies involving Cd(II) ions is presented in Table 1. A full central composite design comprising 30 experiments was used in the investigations. The design consisted of 8 factorial points, 6 star points and 6 replicates to check for consistency of the method employed. The average adsorption efficiency over the 6 replicate runs was 7.34 mg/g with a relative standard deviation of 0.13 mg/g showing consistency of the adsorption method.

Table 1. Central composite design experimental domain.

Parameter	pH	Contact time (min)	Dosage (g)	Initial concentration (mg/L)
Min point	2	5	0.1	5
Mid point	5	122.5	0.65	52.5
Max point	8	240	1.2	100

3.3. Response surface methodology process modelling using a central composite design (CCD).

The experimental variables, the actual experimental results and the predicted results for this investigation are presented in Table 2. A non-transformed general quadratic model (Equation 3) was fitted on the experimental data obtained for the adsorption process. The Least Squares regression results are presented in Table 3. A step-wise regression analysis procedure using Design Expert V11 was conducted to eliminate insignificant terms ($p > 0.05$) [35].

From Table 3, it is quite clear that C, D, AB, AC, AD, BC, BD, CD, C^2, and D^2 are significant model terms ($p < 0.05$) [24,36]. The terms, A and B were retained in the model equation to support hierarchy. The final model is presented by Equation 5.

$$q_e = \beta_0 + \beta_1 A + \beta_2 B + \beta_3 C + \beta_4 D + \beta_5 C^2 + \beta_6 D^2 + \beta_7 AB + \beta_8 AC + \beta_9 AD + \beta_{10} BC + \beta_{11} BD + \beta_{12} CD \quad (5)$$

Table 3 Least Squares regression data for Cd(II) adsorption.

Factor	Coefficient estimate	Coefficient estimate	p-Value
	Actual factors (β)	Coded factors (β)	
Intercept	10.8419	9.31	
A-pH	-0.173	-0.0077	0.985
B-Contact time	-0.0271	0.6142	0.0806
C-Dosage	-23.359	-6.84	< 0.0001
D-Conc	0.2459	6.36	< 0.0001
AB	0.0044	0.6318	0.0054
AC	-0.894	-1.06	0.0062
AD	0.0053	0.6324	0.0381
BC	0.0211	0.5767	0.0104
BD	-0.0001	-0.3942	0.0253
CD	-0.2212	-4.99	< 0.0001
C^2	17.0533	3.85	< 0.0001
D^2	0.0005	1.08	0.0019

Table 2. Experimental variables and results.

Run	Factor 1 pH.	Factor 2 Contact time min	Factor 3 Dosage g	Factor 4 Initial concentration mg/L	Removal R %	Observed q_e mg/g	Predicted q_e mg/g
1	5	122.5	0.65	5	95.6	0.74	0.71
2	3.5	63.75	0.93	28.75	97.04	3.02	2.68
3	5	122.5	0.65	52.5	91.6	7.4	7.3
4	6.5	181.25	0.93	28.75	97.81	3.04	2.96
5	6.5	181.25	0.38	76.25	91.87	18.68	18.75
6	6.5	63.75	0.38	76.25	91.37	18.58	18.93

Run	Factor 1 pH.	Factor 2 Contact time min	Factor 3 Dosage g	Factor 4 Initial concentration mg/L	Removal R %	Observed q_e mg/g	Predicted q_e mg/g
7	5	122.5	1.2	52.5	98.46	4.31	4.38
8	5	122.5	0.65	52.5	92.74	7.49	7.3
9	5	122.5	0.65	100	90.36	13.9	16.06
10	5	122.5	0.65	52.5	90.78	7.33	7.3
11	5	240	0.65	52.5	92.61	7.48	7.43
12	3.5	181.25	0.93	28.75	97.46	3.03	3.11
13	6.5	63.75	0.38	28.75	96.66	7.41	7.59
14	5	122.5	0.38	52.5	91.5	12.81	12.63
15	3.5	63.75	0.65	76.25	90.6	10.63	11.65
16	6.5	181.25	0.93	28.75	94.05	2.92	2.96
17	5	5	0.65	52.5	90.61	7.32	7.18
18	6.5	63.75	0.38	76.25	94.91	19.3	18.93
19	8	122.5	0.65	52.5	91.26	7.37	7.5
20	3.5	181.25	0.38	28.75	90.3	6.92	6.88
21	5	122.5	0.38	52.5	90.72	12.7	12.63
22	3.5	181.25	0.65	76.25	89.19	10.46	10.6
23	3.5	63.75	0.93	28.75	78.75	2.45	2.68
24	5	122.5	0.65	52.5	88.13	7.12	7.3
25	6.5	63.75	0.93	28.75	96.87	3.01	0.98
26	2	122.5	0.65	52.5	84.02	6.79	7.11
27	6.5	181.25	0.93	76.25	92.84	7.65	7.72
28	3.5	181.25	0.93	76.25	89.73	7.4	7.12
29	5	122.5	0.1	52.5	85.24	44.75	20.54
30	3.5	63.75	0.93	76.25	90.01	7.42	7.49

The results of the analysis of variance (ANOVA) for the regression process are presented in Table 4. A p-value of less than 0.05 ($p = 0.0001$) showed that the model was statistically significant [36]. This was further supported by a higher regression coefficient of 0.999. A small variation of 0.0073 between the predicted R^2 (0.9900) and the adjusted R^2 (0.9973) is further evidence for the significance of the model. In addition, the Lack of Fit F-value of 0.785 implied a higher probability of the model fitting the data. Furthermore, an adequate precision greater than 4 is desirable as it measures the signal-to-noise ratio. On the basis of the above results, an adequate precision of 100.68 was obtained showing an adequate signal.

Table 4. ANOVA for response surface quadratic model.

Source	Sum of Squares	Mean Square	F Value	Prob > F
Model			773.86	< 0.0001
Residual	0.8511	0.0655		
Lack of Fit	0.3423	0.057	0.7848	0.6082
Pure Error	0.5089	0.0727		
Cor Total	608.85			
Root MSE	0.0887	R^2	0.9986	
Dep Mean	1.7248	Adj R^2	0.9973	
C.V.	3.21	Pred R^2	0.99	
PRESS	6.44	Adeq Precision	100.6836	Desire > 4

3.4. Model validation.

Before being used in interpreting the experimental data, the quadratic model was validated based on the normal probability graph, plot of standard residuals versus the predicted values, absence of outliers and a plot of experimental data versus predicted data [37]. The normal probability plot showed normally distributed data as evidenced by random distribution of data around and along the oblique line (graph not shown). This is further supported by random distribution of residuals around the zero line and absence of outliers (outside the defined boundaries) in Fig 4a. Moreover, a small variance between the experimental and predicted values in Fig 4b is further evidence of the validity of the predictive model.

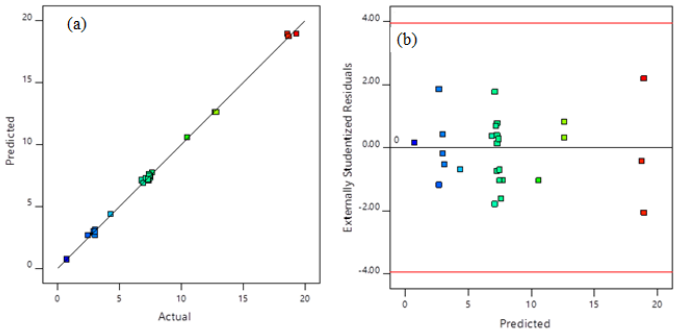

Figure 4. Plot of standard residuals versus the predicted values (a) Plot of experimental data versus predicted data (b).

3.5 Model interpretation.

Evaluation of the influence of the independent variables on adsorption efficiency of the adsorbent was conducted by analysing 3-Dimensional surface plots. Fig. 5a shows the effect of pH and contact time on Cd(II) ions adsorption efficiency at constant dosage and initial Cd(II) concentration. An increase in both pH and contact time enhanced the Cd(II) ions adsorption efficiency. Solution pH affects both the metal ions and the ionisation of the functional groups present on the surface of the adsorbent. Initially, the adsorbent had abundant binding sites

which were occupied gradually as time progressed and hence a gradual increase in adsorption efficiency [11]. At low pH, there is competition between Cd(II) ions and the more available protons This competition for active sites results in low Cd(II) adsorption efficiency. However, as pH increases, concentration of the protons decreases and hence an increase in adsorption efficiency. The optimum pH was 5.29 which is in agreement with the obtained pHzpc 5.43 of the adsorbent. At pHs beyond the pHzpc, Cd(II) tends to precipitate and hence a continued increase in adsorption efficiency.

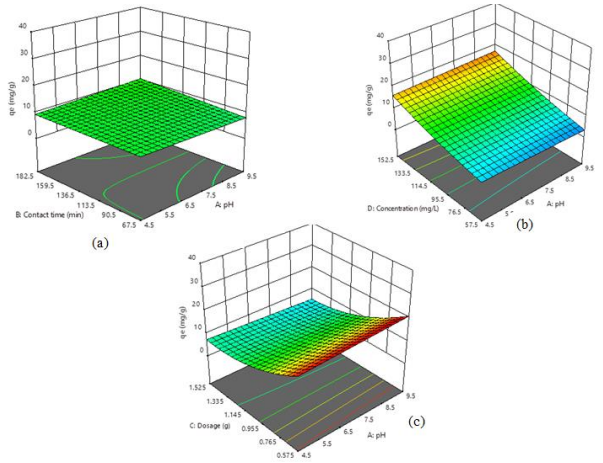

Figure 5. 3-D surface plot for the combined effect of pH and contact time (a), pH and Initial concentration (b), pH and dosage (c), on Cd(II) adsorption efficiency.

Fig. 5(b) shows the effect of pH and initial Cd(II) concentration on Cd(II) ions adsorption efficiency at specified conditions. There was a notable decrease in adsorption efficiency with decrease in initial Cd(II) concentration at low pH. Functional groups on the surface of the adsorbent such as amine are easily protonated whilst carboxylic groups retain their protons at low pH. This reduces electrostatic interactions between the adsorbent and Cd(II) ions and hence low adsorption efficiency [11].

Fig. 5(c) shows the effect of pH and dosage on Cd(II) ions adsorption efficiency. High adsorption efficiency can be noticed at low dosages as more active sites would be available for adsorption process. A notable decrease in adsorption efficiency as adsorbent dosage was increased could be attributed to overlapping of the active sites as a result of excess adsorbent dosage.

3.6. Optimisation of the adsorption process.

The desirability function on the Design Expert software was used to determine Cd(II) adsorption efficiency and the optimum experimental conditions [38]. The optimum conditions were determined to be pH 5.29, contact time (67.50 min), dosage (0.575 g) and initial concentration (152.50 mg/L) giving a maximum Cd(II) removal capacity of 32.06 mg/g. The optimum conditions were confirmed by carrying 6 replica runs at room temperature and the Cd(II) adsorption efficiency was deduced to be 30.45 ± 0.87 mg/g.

3.7. Isotherm studies.

In the current study, the Langmuir [39], Freundlich [40], and Temkin [38] isotherms were applied in interpretation of adsorption experimental data. The correlation coefficients of the models were used in deciding the best fitting model (Table 5).

Table 5 Langmuir, Freundlich and Temkin parameters for Cd(II) adsorption.

Isotherm	Parameter	Cd(II)
Langmuir	q_{max} (mg g^{-1})	188.68
	b (L mg^{-1})	0.001
	R_L	0.927-0.996
	R^2	0.998
Freundlich	K_F (mg g^{-1})	8.55
	n	0.949
	R^2	0.996
Temkin	b	321.35
	K_T (L mg^{-1})	16.19
	R^2	0.892
	B_1	7.71

The linear Langmuir isotherm model is represented by Equation 6.

$$\frac{1}{q_e} = \frac{1}{q_{max}} + \left(\frac{1}{bq_{max}}\right)\frac{1}{C_e} \qquad (6)$$

where q_e is the amount of Cd(II) ions adsorbed at equilibrium, q_{max} is the maximum adsorption capacity in mg/g, C_e is the equilibrium concentration in mg/L, and b is the equilibrium Langmuir constant.

The Langmuir plot is presented in Fig 6a. Fitting of the model was done in excel using the solver package to optimise the Langmuir parameters. The correlation coefficient together with the sum of square deviation shows that the Langmuir model best represented the isotherm behavior of the adsorption process relative to the Freundlich model (Table 5). The maximum adsorption capacity of the hybrid adsorbent was deduced to be 188.68 mg/g.

The linear form of the Freundlich isotherm is given by Equation 7.

$$\ln q_e = \ln K_F + \frac{1}{n}\ln C_e \qquad (7)$$

where q_e (mg/g) is the amount of Cd(II) ions adsorbed at equilibrium by the adsorbent, K_F (mg/g) represents the adsorption capacity, C_e (mg/L) is the equilibrium concentration and n is the intensity of adsorption. The Freundlich linear plot is shown in Fig 6b. Relative to the Langmuir model, the Freundlich model could not fit better the isotherm data as evidenced by lower coefficient of determination (R^2=0.996).

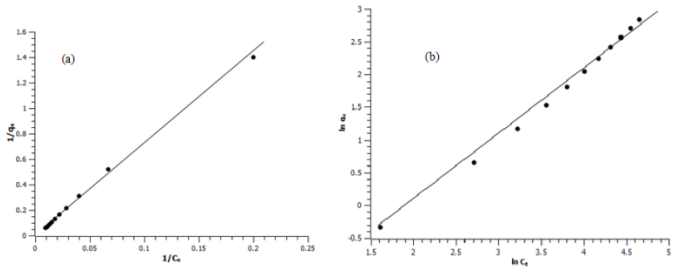

Figure 6. Langmuir (a), Freundlich (b) adsorption isotherms for Cd(II) onto TAC-MH (pH 5, dosage concentration 6.5 g/L, contact time 122.5 min, initial concentration 5 – 105 mg/L, temperature 20 ºC).

The Temkin isotherm model was also applied in analysing the equilibrium data. The Temkin model is given by Equation 8.

$$q_e = B_1 \ln K_T + B_1 \ln C_e \qquad (8)$$

where, $B_1 = \frac{RT}{b}$, R is the universal gas constant (J $mol^{-1}K^{-1}$), T is the absolute temperature (Kelvin), b is the Temkin constant related to the heat of adsorption and K_T is the equilibrium binding constant (L mg^{-1}) corresponding to the maximum binding energy.

Of the three isotherm models applied to the isotherm data, the Langmuir model (Table 5) best described the nature of the adsorption process and hence could be concluded that the adsorption process was monolayer [41].

3.8. Adsorption kinetics.

Kinetic data were modelled using different kinetic models including pseudo-first-order kinetic model and pseudo-second-order kinetic model. The pseudo-first-order kinetic model is expressed in linear form by Lagergren [42] as follows:

$$\log\ (q_e - q_t) = \log q_e - \frac{t.\ k_1}{2.3} \quad (9)$$

where, q_t and q_e are the amount of Cd(II) ions adsorbed in mg g^{-1} at any time t and at equilibrium, respectively, k_1 (min^{-1}) is the rate constant and t is the time (min). Parameter values of k_1 (0.0099 min^{-1}) and q_e (2.901 mg g^{-1}) were estimated from the slope and the intercept, respectively of a plot of log ($q_e - q_t$) versus t (Fig. 7a).

The model parameters are presented in Table 6.

The kinetic data obtained was further subjected to pseudo-second-order kinetic modelling. The second order kinetic model is expressed in linear form by Equation 10.

$$\frac{t}{q_t} = \frac{t}{q_e} + \frac{1}{k_2(q_e)^2} \quad (10)$$

where k_2 is the equilibrium rate constant (g mg^{-1} min^{-1}). The values of q_e and $k_2$were deduced from the slope and intercept of the plot of (t/q_t) versus t, respectively (Fig. 7b).The second order kinetic parameters are presented in Table 6.

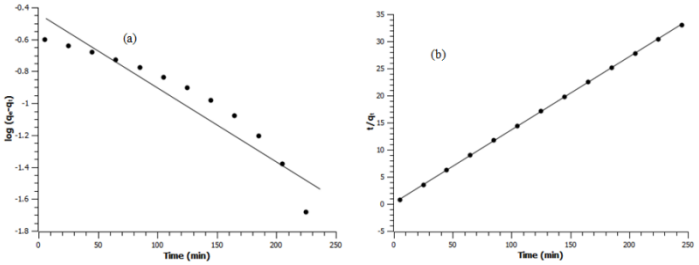

Figure 7. Pseudo-first-order kinetic (a) and pseudo-second-order kinetic (b) plots for the adsorption of Cd(II) (pH 5, initial concentration 52.5 mg/L, dosage concentration 6.5 g/L, time 5 - 245 min).

The pseudo-first-order kinetic correlation coefficient was found to be lower (R^2 = 0.895) relative to that of the pseudo-second-order kinetic model indicating that the first order model could not satisfactorily describe the kinetics of Cd(II) adsorption onto the hybrid adsorbent. The pseudo-second-order could describe the kinetic better as evidenced by relatively higher correlation coefficient (R^2=0.999). Moreover, the second-order $q_{e,\ calculated}$ value (7.435 mg/g) was in better agreement with its $q_{e,\ experimental}$ value (7.432 mg/g). These results are consistent with an adsorption process which depended on concentration and thus the rate determining step involved chemical adsorption.

The intra-particle diffusion model is expressed as follows:

$$q_e = I + K_i t^{0.5} \quad (11)$$

where *I* is the thickness of the boundary layer and K_i is the rate constant for the intra-particle diffusion (mg g^{-1} $min^{-1/2}$). A plot of q_e versus $t^{0.5}$ (Fig not shown) was used to estimate *I* and K_i (Table 6) values. The plot did not pass through the origin showing some level of boundary layer control. This further showed that there were other kinetic models controlling the adsorption rate hence the intra-particle diffusion was not the only rate limiting step [43].

3.9. Adsorption thermodynamics.

The influence of temperature on the adsorption process was investigated with the intention to understand the thermodynamic behavior of the process. The thermodynamic parameters which include entropy change (ΔS^o), enthalpy change (ΔH^o) and the standard Gibb's free energy change (ΔG^o), were estimated from equations 12-15.

$$K_c = \frac{q_e}{C_e} \quad (12)$$

$$\Delta G^o = -RT \ln K_c \quad (13)$$

$$\Delta G^o = \Delta H^o - T\Delta S^o \quad (14)$$

$$\ln K_c = \frac{\Delta S^o}{R} + \frac{\Delta H^o}{RT} \quad (15)$$

Where, K_c is the thermodynamic equilibrium constant, q_e is the amount of Cd(II) adsorbed at equilibrium in mg/L, C_e is the equilibrium concentration of Cd(II) ions in solution, R is the ideal gas constant and T is the temperature in K.

The ΔH^o and ΔS^o were calculated from slope and intercept of plot ln K_d versus 1/T,, respectively. The ΔG^o values were -4.438,-4.872, -5.306 and -5.740 kJ/mol at 293.15, 303.15, 313.15 and 323.15 K, respectively. The negative values show that the adsorption process was feasible and spontaneous. The positive ΔH^o (+8.285 kJ/mol) value shows that the Cd(II) adsorption by the adsorbent was endothermic and was favored at elevated temperatures. Randomness at the solid/solution interface was evidenced by the positive ΔS^o (+0.0434 kJ/mol) value.

Table 6. Kinetic parameters for Cd(II) adsorption.

Experimental value	Pseudo-first-order kinetic model			Pseudo-second-order kinetic model			Intraparticle diffusion model	
q_e	q_e	k_1	R^2	q_e	k_2	R^2	K_{iff}	R^2
(mg g^{-1})	(mg g^{-1})	(min^{-1})		(mg g^{-1})	(g mg^{-1} min^{-1})		(mg g^{-1} $t^{-1/2}$)	
7.432	2.901	0.0099	0.895	7.435	0.093	0.999	0.0195	0.9571

3.10. Comparison of TAC-MH with other magnetic adsorbents.

The prepared adsorbent (TAC-MH) was compared to other adsorbents with respect to maximum monolayer adsorption capacity and the comparison results are presented in Table 7.

May it be noted that maximum adsorption capacities vary as they depend on the extent of surface modification, characteristics of an individual adsorbent, heat treatment temperatures, the analytical method used for decontamination and the initial concentration of the adsorbate used. Relative to previous adsorbents we fabricated and others reported in literature, TAC-MH showed a reasonable and competitive adsorption capability which makes it a promising candidate Cd(II) adsorption. Furthermore, the precursor used in fabrication of this adsorbent, maize tassel is an agricultural waste which is cheap and always available in abundance.

Table 7 Maximum adsorption capacities of Cd(II) from aqueous media using various sorbents

Sorbents	q_{max} (mg g^{-1})	References
Akagabeite nanocrystals	17.1	[44]
Orange peel–Fe_2O_3 (MNP–OPP)	71.3	[45]
Fe_3O_4@APS@AA-co-CA MNPs	29.6	[46]
Magnetic Fe_3O_4 baker's yeast biomass	41	[47]
SDS modified magnetite nanoparticles	9.6	[43]
MT-MN	52.05	[17]
Fe_3O_4/cyclodextrin polymer nanocomposites	27.7	[48]
TAC-MH	188.68	This study

3.11. Desorption studies.

Adsorbent material regeneration and reusability studies are critical in evaluating the practical applicability of the material. Adsorption-desorption process cycles were carried out to determine the feasibility of regenerating and reusing a spent adsorbent. Even after 5 adsorption-desorption cycles, the adsorption efficiency of the adsorbent kept being above 80% (Fig 8). This is strong evidence for potential applicability of the adsorbent material in real life situations.

3.12. Application of the adsorbent in real effluent samples.

TAC-MH was applied in treatment of effluent from local industry. The effluent was analyzed prior to treatment with the adsorbent employing the optimized process conditions. The results of effluent analysis before and after treatment are presented in Table 8. It can be noted that Cd(II) ions were significantly decreased in effluent by 85.83%. Other species present in effluent were notably decreased showing that TAC-MH is a good candidate for treatment of Cd(II) contaminated wastewaters.

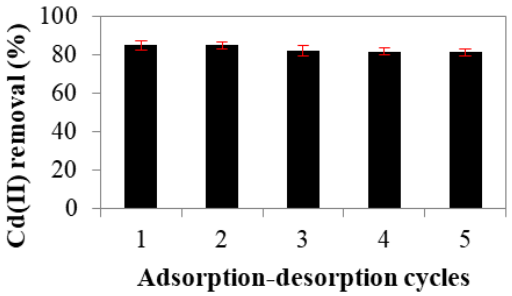

Figure 8. Adsorbent regeneration through adsorption-desorption studies.

Table 8. Effluent analysis.

Parameter	Before adsorption	After adsorption
Cd Concentration (mg/L)	3.97	0.563
pH	2.5	2.5
Conductivity	76.1	70
Chlorides (mg/L)	2849.1	149.95
Pb concentrations (mg/L)	5.5	1.4

4. CONCLUSIONS

The present study shows that TAC-MH has much potential as an adsorbent for the removal of Cd(II) from aqueous solution. The influences of pH, adsorbent dosage, contact time, and initial concentration on adsorption of the metal ion and their interactions were investigated by a response surface methodology and ANOVA. The desirability function optimization showed that the optimum removal capacity (32.06 mg/g was obtained at a pH, contact time, adsorbent dosage and initial Cd(II) concentration of 5.9, 67.50 min, 0.575 g and 152.50 mg/L, respectively. Confirmatory experimental analysis under the optimized conditions gave an average Cd(II) removal capacity of 30.45 ± 0.87 mg/g. The Langmuir isotherm model best described the adsorption mechanism with a maximum adsorption capacity of 188.68 mg/g. The kinetic study was performed based on pseudo-first-order, pseudo-second-order and intraparticle diffusion equations. The results show that the adsorption follows pseudo-second-order in addition to intraparticle diffusion model. The results obtained in the present work showed that the TAC-MH can be used as an effective adsorbent for removal Cd(II) ions from aqueous solution.

5. REFERENCES

1. Badr, Y.; El-Wahed, M.G.A.; Mahmoud, M.A. Photocatalytic degradation of methyl red dye by silica nanoparticles. *J. Hazard Mater.* **2008**, *154*, 245–253, https://doi.org/10.1016/j.jhazmat.2007.10.020 .
2. Ji, K.; Kim, J.; Lee, M.; Park, S.; Kwon, H.J.; Cheong, H.K.; Jang, J.Y.; Kim, D.S.; Yu, S.; Kim, Y.W.; Lee, K.Y.; Yang, S.O.; Jhung, I.J.; Yang, W.H.; Paek, Y.C.; Hong, Y.C.; Choi, K. Assessment of exposure to heavy metals and health risks among residents near abandoned metal mines in Goseong. *Korea. Environ. Pollut.* **2013**, *178*, 322–8, https://doi.org/10.1016/j.envpol.2013.03.031.
3. Xu, P.; Zeng, G.M.; Huang, D.L.; Lai, C.; Zhao, M.H.; Wei, Z.; Li, N.J.; Huang, C.; Xie, G.X. Adsorption of Pb(II) by iron oxide nanoparticles immobilized Phanerochaete chrysosporium: Equilibrium, kinetic, thermodynamic and mechanisms analysis. *Chem. Eng. J.* **2012,** *203*, 423–431, https://doi.org/10.1016/j.cej.2012.07.048.
4. Zhao, W.; Tang, Y.; Xi, J.; Kong, J. Functionalized graphene sheets with poly(ionic liquid)s and high adsorption capacity of anionic dyes. *Appl. Surf. Sci.* **2015**, *326*, 276–284, https://doi.org/10.1016/j.apsusc.2014.11.069.
5. Obregón-Valencia, D.; Sun-Kou, R. Comparative cadmium adsorption study on activated carbon prepared from aguaje (Mauritia flexuosa) and olive fruit stones (Olea europaea L.). *J. Environ. Chem. Eng.* **2014**, *2*, 2280–2288, https://doi.org/10.1016/j.jece.2014.10.004.
6. World Health Organisation. Guidelines for Drinking-water Quality, 2006.
7. Qu, J.; Meng, X.; You, H.; Ye, X.; Du, Z. Utilization of rice husks functionalized with xanthates as cost-effective biosorbents for optimal Cd(II) removal from aqueous solution via response surface methodology. *Bioresour. Technol.* **2017**, *214*, 1036-1042, https://doi.org/10.1016/j.biortech.2017.06.055.
8. Sikder, T.; Fujita, S. Facile synthesis , characterization , and adsorption properties of Cd (II) from aqueous solution using β -cyclodextrin polymer impregnated in functionalized chitosan beads as a novel adsorbent. *J. Environ. Chem. Eng.* **2017**, *5*, 3395–3404.

9. Chen, J.P.; Yang, L. Chemical Modification of Sargassum sp. for Prevention of Organic Leaching and Enhancement of Uptake during Metal Biosorption. *Ind. Eng. Chem. Res.* **2005**, *44*, 9931–9942, https://doi.org/10.1021/ie050678t.
10. Guo, Z.; Zhang, X.; Kang, Y.; Zhang, J. Biomass-Derived Carbon Sorbents for Cd(II) Removal: Activation and Adsorption Mechanism. *Am. Chem. Soc. Sustain. Chem. Eng*. **2017**, *5*, 4103–4109, https://doi.org/10.1021/acssuschemeng.7b00061.
11. Nethaji, S.; Sivasamy, A.; Mandal, A.B. Preparation and characterisation of corn cob activated carbon coated with nano-sized magnetite particles for the removal of Cr(VI). *Bioresour. Technol.* **2013**, *134*, 94–100, https://doi.org/10.1016/j.biortech.2013.02.012.
12. Ghaedi, M.; Shokrollahi, A.; Tavallali, H.; Shojaiepoor, F.; Keshavarz, B.; Hossainian, H,; Soylak, M.; Purkait, M.K. Activated carbon and multiwalled carbon nanotubes as efficient adsorbents for removal of arsenazo(III) and methyl red from wastewater. *Toxicol. Environ. Chem*. **2011**, *93*, 438–449, https://doi.org/10.1080/02772248.2010.540244.
13. Rao, G.P.; Lu, C.; Su, F. Sorption of divalent metal ions from aqueous solution by carbon nanotubes: A review. *Sep. Purif. Technol*. **2007**, *58*, 224–231, https://doi.org/10.1016/j.seppur.2006.12.006.
14. Gupta, V.K.; Agarwal, S.; Saleh, T.A. Chromium removal by combining the magnetic properties of iron oxide with adsorption properties of carbon nanotubes. *Water Res*. **2011**, *45*, 2207–2212, https://doi.org/10.1016/j.watres.2011.01.012.
15. Ai, L.; Zhang, C.; Liao, F. Removal of methylene blue from aqueous solution with magnetite loaded multi-wall carbon nanotube: kinetic, isotherm and mechanism analysis. *J. Hazard Mater*. **2011**, *198*, 282–290, https://doi.org/10.1016/j.jhazmat.2011.10.041.
16. Guyo, U.; Makawa, T.; Moyo, M.; Nharingo, T.; Nyamuda, B.C.; Mugadza, T. Application of response surface methodology for Cd (II) adsorption on maize tassel-magnetite nanohybrid adsorbent. *J. Environ. Chem. Eng.* **2017**, *3*, 2472–2483, https://doi.org/10.1016/j.jece.2015.09.006.
17. Liu, H.; Peng, S.; Shu, L.; Chen, T.; Bao, T.; Frost, R.L. Magnetic zeolite NaA: Synthesis,characterization based on metakaolin and its application for the removal of Cu^{2+}, Pb^{2+}. *Chemosphere*. **2013**, *91*, 1539–1546, https://doi.org/10.1016/j.chemosphere.2012.12.038.
18. Singh, K.; Gupta, S.; Singh, A.; Sinha, S. Optimizing adsorption of crystal violet dye from water by magnetic nanocomposite using response surface modeling approach. *J. Hazard Mater. 186*, 1462–1473, **2011**, https://doi.org/10.1016/j.jhazmat.2010.12.032.
19. Duran, A.; Soylak, M.; Tuncel, S.A. Poly(vinyl pyridine-poly ethylene glycol methacrylate-ethylene glycol dimethacrylate) beads for heavy metal removal. *J. Hazard Mater*. **2008**, *155*, 114–20, https://doi.org/10.1016/j.jhazmat.2007.11.037.
20. Hsu, S.T.; Chen, L.C.; Lee, C.C.; Pan, T.C.; You, B.X.; Yan, Q.F. Preparation of methacrylic acid-modified rice husk improved by an experimental design and application for paraquat adsorption. *J. Hazard Mater*. **2009**, *171*, 465–470, https://doi.org/10.1016/j.jhazmat.2009.06.144.
21. Moyo, M.; Chikazaza, L.; Nyamunda, B.C.; Guyo, U. Adsorption Batch Studies on the Removal of Pb (II) Using Maize Tassel Based Activated Carbon. *J. Chem.* **2013**, 2013, 1-8, http://dx.doi.org/10.1155/2013/508934.
22. Gu, W.; Sun, C.J.; Liu, Q.; Cui, H.X. Adsorption of avermectins on activated carbon: Equilibrium, kinetics, and UV-shielding. *Trans. Nonferrous Met. Soc. China*, **2009**, 19, 845–850, https://doi.org/10.1016/S1003-6326(10)60163-X.
23. Gedam, A.H.; Dongre, R.S. Activated carbon from Luffa cylindrica doped chitosan for mitigation of lead(ii) from an aqueous solution. *RSC Adv.* **2016,** *6*, 22639–22652, https://doi.org/10.1039/C5RA22580A.
24. Fakhri, A.; Rashidi, S.; Tyagi, I.; Agarwal, S.; Gupta, V.K. Photodegradation of Erythromycin antibiotic by γ-Fe2O3/SiO2 nanocomposite: Response surface methodology modeling and optimization. *J. Mol. Liquids.* **2016**, *214*, 378-383, https://doi.org/10.1016/j.molliq.2015.11.037.
25. Salehi, P.; Tajabadi, F.M.; Younesi, H.; Dasht,i Y. Optimization of lead and nickel biosorption by Cystoseira trinodis (brown algae) using response surface methodology. *Clean - Soil, Air, Water* **2014**, *42*, 243–250, https://doi.org/10.1002/clen.201100429.
26. Savasari, M.; Emadi, M.; Bahmanyar, M.A.; Biparva, P. Optimization of Cd (II) removal fromaqueous solution by ascorbic acidstabilized zero valent iron nanoparticles using response surface methodology. *J. Ind. Eng. Chem*. **2015**, *21*, 1403-1409, https://doi.org/10.1016/j.jiec.2014.06.014.
27. Zhu, H.; Fu, Y.; Jiang, R.; Yao, J.; Xiao, L.; Zeng, G. Optimization of copper (II) adsorption onto novel magnetic calcium alginate/maghemite hydrogel beads using response surface methodology. *Ind. Eng. Chem. Res*. **2014**, *53*, 4059–4066, https://doi.org/10.1021/ie4031677.
28. Tian, Y.; Wu, M.; Lin, X.; Huang, P.; Huang, Y. Synthesis of magnetic wheat straw for arsenic adsorption. *J. Hazard Mater*. **2011**, *193*, 10–16, https://doi.org/10.1016/j.jhazmat.2011.04.093.
29. Zhu, M.; Zhu, L.; Wang, J.; Yue, T.; Li, R.; Li, Z. Adsorption of Cd (II) and Pb (II) by in situ oxidized Fe_3O_4 membrane grafted on 316L porous stainless steel fi lter tube and its potential application for drinking water treatment. *J. Environ. Manage* **2017**, *196*, 127–136, https://doi.org/10.1016/j.jhazmat.2011.04.093.
30. Oickle, A.M.; Tarasuk, A.C.; Goertzen, S.L.; Theriault, K.D.; Andreas, H.A. Standardization of the Boehm titration . Part I . CO_2 expulsion and endpoint determination. *Carbon* **2010**, *48*, 1252–1261, https://doi.org/10.1016/j.carbon.2009.11.050.
31. Dada, A.O.; Ojediran, J.O.; Olalekan, A.P. Sorption of Pb^{2+} from aqueous solution unto modified rice husk: isotherms studies. *Adv. Phys. Chem., 2013*, http://dx.doi.org/10.1155/2013/842425.
32. Nath, K.; Panchani, S.; Bhakhar, M.S.; Chatrola, S. Preparation of activated carbon from dried pods of Prosopis cineraria with zinc chloride activation for the removal of phenol. *Environ. Sci. Pollut. Res*. **2013**, *20*, 4030–4045, https://doi.org/10.1007/s11356-012-1325-y.
33. Jackson, M.; Mantsch, H.H. The Use and Misuse of FTIR Spectroscopy in the Determination of Protein Structure. *Crit. Rev. Biochem. Mol. Biol*. **1995,** *30*, 95-120, https://doi.org/10.3109/10409239509085140.
34. . Moyo, M.; Nyamhere, G.; Sebata, E.; Guyo, U. Kinetic and equilibrium modelling of lead sorption from aqueous solution by activated carbon from goat dung. *Desalin. Water Treat* **2014**, 1–11, https://doi.org/10.1080/19443994.2014.968217.
35. Montgomery, D.; Peck, E.; Vining, G. *Introduction to linear regression analysis.* John Wiley & Sons, 2012.
36. Fakhri, A. Application of response surface methodology to optimize the process variables for fluoride ion removal using

maghemite nanoparticles. *J. Saudi Chem. Soc.* **2014**, *183*, 340–347, https://doi.org/10.1016/j.jscs.2013.10.010.
37. Cameron, A.; Trivedi, P. *Regression analysis of count data*. Cambridge University Press, 2013; https://doi.org/10.1017/CBO9781139013567.
38. Roosta M., Ghaedi M., Daneshfar A., et al., Optimization of the ultrasonic assisted removal of methylene blue by gold nanoparticles loaded on activated carbon using experimental design methodology. *Ultrason. Sonochem*. **2013**, *21*, 242–252, https://doi.org/10.1016/j.ultsonch.2013.05.014.
39. Langmuir, I. The Constitution and Fundamental Properties of Solids and Liquids-Part 1: Solids. *J. Am. Chem. Soc*. **1916**, *38*, 2221–2295, https://doi.org/10.1021/ja02268a002
40. Freundlich, H.M. Over the adsorption in solution. *J. Phys. Chem*. **1906**, *57*, 384–470.
41. Ghaedi, M.; Ansari, A.; Habibi, M.H.; Asghari, A.R. Removal of malachite green from aqueous solution by zinc oxide nanoparticle loaded on activated carbon : Kinetics and isotherm study. *J. Ind. Eng. Chem*. **2014**, *21*, 17–28, https://doi.org/10.1016/j.jiec.2013.04.031.
42. Ho, Y.; McKay, G. Pseudo second order model for sorption processes. *Process Biochem.* **1999**, *34*, 451–465, https://doi.org/10.1016/S0032-9592(98)00112-5.
43. Bahrami, M.; Brumand-Nasab, S.; Kashkooli, H.; Firouzi, A.F.; Babaei, A.A. Cadmium Removal from Aqueous Solutions Using Modified Magnetite Nanoparticles. *Iran J. Heal. Environ.* **2013**, *6*, 221–232.
44. Deliyanni, E.A.; Matis, K.A. Sorption of Cd ions onto akaganéite-type nanocrystals. *Sep. Purif. Technol*. **2005**, *45*, 96–102, https://doi.org/10.1016/j.seppur.2005.02.012.
45. Gupta, V.K.; Nayak, A. Cadmium removal and recovery from aqueous solutions by novel adsorbents prepared from orange peel and Fe_2O_3 nanoparticles. *Chem. Eng. J.* **2012,** *180*, 81– 90, https://doi.org/10.1016/j.cej.2011.11.006.
46. Ge, F.; Li, M.M.; Ye, H.; Zhao, B.X. Effective removal of heavy metal ions Cd^{2+}, Zn^{2+}, Pb^{2+}, Cu^{2+} from aqueous solution by polymer-modified magnetic nanoparticles. *J. Hazard Mater.* **2012**, *211-212*, 366–372, https://doi.org/10.1016/j.jhazmat.2011.12.013.
47. Xu, M.; Zhang, Y.; Zhang, Z.; Shen, Y. Study on the adsorption of Ca^{2+}, Cd^{2+} and Pb^{2+} by magnetic Fe_3O_4 yeast treated with EDTA dianhydride. *Chem. Eng. J*. **2011,** *168*, 737–745, https://doi.org/10.1016/j.cej.2011.01.069.
48. Badruddoza, A.Z.M.; Shawon, Z.B.Z.; Tay, W.J.D.; Hidajat, K.; Uddin, M.S. Fe_3O_4/cyclodextrin polymer nanocomposites for selective heavy metals removal from industrial wastewater. *Carbohydr. Polym*. **2013,** *91*, 322–332, https://doi.org/10.1016/j.carbpol.2012.08.030.

6. ACKNOWLEDGEMENTS

The authors appreciate contribution by the Midlands State University Research and Postgraduate Studies Office for funding the research activities.